Theor Appl Climatol (2014) 116:273–285
DOI 10.1007/s00704-013-0952-7

ORIGINAL PAPER

A modification of HASM for interpolating precipitation in China

Na Zhao · Tianxiang Yue

Received: 1 April 2013 / Accepted: 11 June 2013 / Published online: 5 July 2013

Abstract Based on the spatial distribution of precipitation in China, this study gives a modification of High Accuracy Surface Modeling (HASM) method for improving interpolation of precipitation. To assess the feasibility of this modified model, namely, HASM-PRE, we use precipitation data measured at 712 stations for the period 1951–2010, using 605 stations for function development and reserving 107 for validation tests. The performance of HASM-PRE is compared with those of HASM and other classical methods: kriging, inverse distance weighted (IDW) method and spline. Results show that HASM-PRE has less root mean square error (RMSE) and mean absolute error (MAE) than the other techniques tested in this study. The precipitation map obtained from HASM-PRE is better than that obtained using other methods. Therefore, HASM-PRE can be seen as an alternative to the popular interpolation techniques, particularly if we focus on simulation accuracy. In addition, the effective way to combine the strengths of both human expert and differential geometry in this study can be applied for calculating precipitation for other areas in other temporal scales. For better improvement, HASM-PRE can be combined with ancillary variables and implemented in parallel environments.

1 Introduction

Spatially distributed estimations of precipitation are required as inputs to many environmental models (Xu and Singh 1998; Vieux 2001; Smith et al. 2001; Hasenauer et al. 2003; Sato et al. 2004; Robertson et al. 2007; Tong and Naramngam 2007; Rowhani et al. 2011). However, in most cases, the networks of the precipitation measuring stations are sparse and the available data are insufficient to characterize the highly variable precipitation and its spatial distribution. Therefore, it is necessary to find methods to estimate precipitation in areas where precipitation has not been measured. Interpolation is a way of reconstructing continuous fields from variables measured at point locations. Many interpolation techniques are used to interpolate climate variables (Daly et al. 1994, 2001, 2002; Goovaerts 2000; Yan et al. 2005; Ninyerola et al. 2007; Teegavarapu 2007; DeGaetano and Wilks 2009; Portales et al. 2010). However, there is no optimum method to define the surface of mean precipitation especially in an area of complex climatology. The optimal interpolation method should be obtained by analyzing the data and the spatial structure (MacEachren and Davidson 1987; Burrough and McDonnell 1998; Brus and Heuvelink 2007; Aalto et al. 2012).

In order to solve the error problem that had long troubled the interpolation method, Yue (2011) developed a novel surface modeling method, High Accuracy Surface Modeling (HASM), based on the fundamental theorem of surface theory. Numerical tests have shown that HASM is much more accurate than the classical methods such as kriging, inverse distance weighted (IDW) method, and spline (Yue and Du 2006; Yue et al. 2007). Surface modeling of digital elevation model (DEM) and ecosystem change also indicate that HASM has increased interpolation accuracy (Yue 2011; Yue et al. 2011). Despite the good performance of HASM from numerical tests and interpolation of some real-world applications, its performance in interpolating precipitation has not been satisfactory.

To improve HASM's simulation skills in interpolating precipitation in China, this research gives a modification of HASM based on the spatial distribution of precipitation in China. We denote the new version of HASM as HASM-PRE, and apply it to simulate mean annual precipitation of China during 1951 to 2010 since long-term climate datasets are often required in many biotic and abiotic processes (Fronzek et al. 2006; Kullmann 2010). The simulation accuracy of HASM-PRE is compared with that of its earlier version (HASM), and the other frequently used interpolators: kriging,

N. Zhao · T. Yue (✉)
State Key Laboratory of Resources and Environmental Information System, Institute of Geographic Sciences and Natural Resources Research, Chinese Academy of Sciences, Beijing 100101, China
e-mail: yue@lreis.ac.cn

IDW and spline, which have been the most widely used methods in climate research (Hevesi et al. 1992; Phillips et al. 1992; Hutchinson 1995; Thornton et al. 1997; Dingman et al. 1998; Hijmans et al. 2006; Samanta et al. 2012).

2 Data and study area

2.1 Data used

Long-term climate observation data are obtained from the national meteorological network in China for the period 1951–2010. China area has a low measurement network density formed of over 750 rain gauges in an areas of approximately 960,000 km^2. The sampling periods of these meteorology stations are not synchronous. Only 712 stations with more than 35 complete years are selected with the exception of 30 locations with between 25 and 35 complete years, which are located in the west of China. Climate site density is higher in eastern China than in western China, and these stations are distributed unevenly (Fig. 1).

2.2 Study area and environmental conditions

The studied area, China (3°51′N–53°33′N, 73°33′E–135°05′E), lies in the southeastern part of the Eurasian Continent, the greatest continent in the world, and lies to the west of the Pacific, the world's largest ocean. China's topography varies greatly from high mountainous regions to inhospitable desert zones and flat, fertile plains. It can be compared to a staircase descending from west to east. In China, climatic control through land and water must be strongly considered, due to the vast continental extent of China itself, on the one hand, and due to the huge extent of both continental and maritime surroundings, on the other. The Indian Ocean may only marginally affect the climate of China, since the Himalayas represents a significant barrier to the influences from the Indian Ocean. Therefore, continental and oceanic effects on the climate of China may vary gradually, from strong oceanic influences over the sea and coastal areas to strong continental influences in the most inland and remote areas in the northwest of China. Abundant atmospheric water vapor mainly comes from the oceans. The monsoon system, together with the effects of topography, yields a remarkable change in annual total precipitation, from less than 25 mm in the northwest to more than 2,000 mm in the southeast, thus representing an increasing precipitation pattern from northwest to southeast over China (Domroes and Peng 1988). From the geostatistics viewpoint, this can be seen as the spatial autocorrelation, which is a very common feature for geographical variables and datasets, and means that observations close to each other are more likely to be similar.

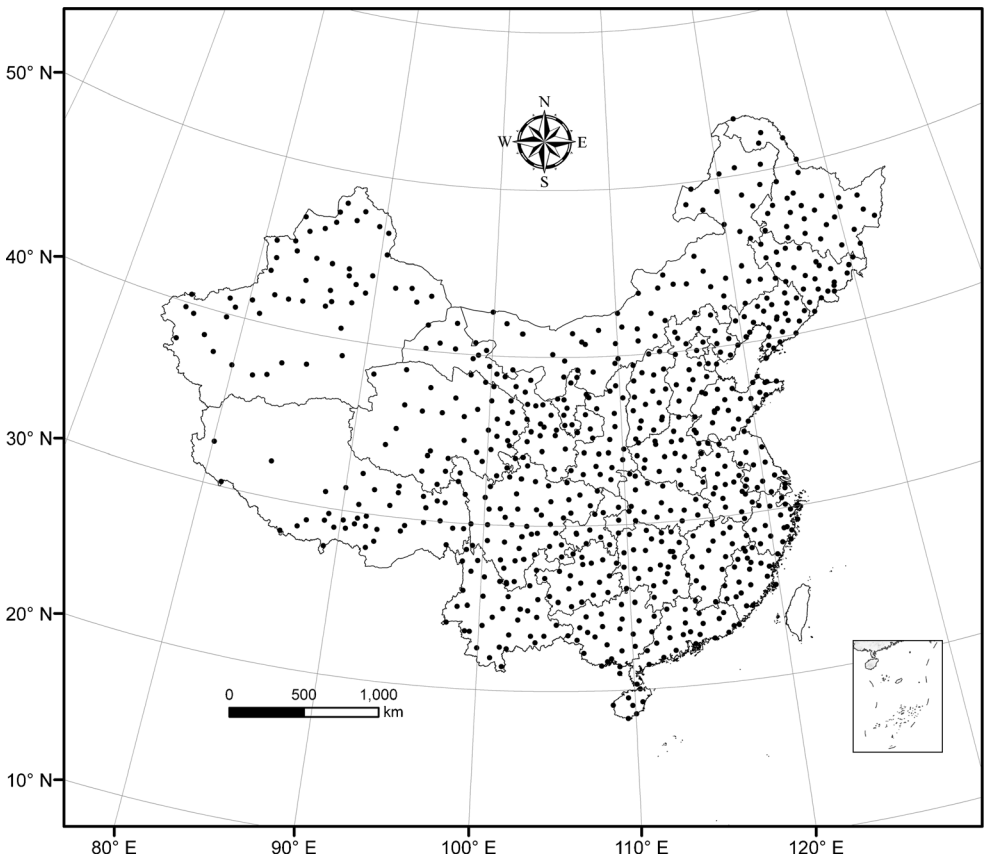

Fig. 1 Spatial distribution of the meteorological network in China

3 Methods

3.1 HASM

As an innovative method, HASM is based on the fundamental theorem of surfaces which makes sure that a surface is uniquely defined by the first and the second fundamental coefficients of it (Henderson 1998). In this section, the fundamental intuition of HASM and its processes are given briefly.

Suppose a surface is a graph of a function $z = f(x, y)$; the first fundamental coefficients indicate how the surface inherits the natural inner product of R^3, in which $R^3$is the set of triples $(x, y, z)$of real numbers (Carmo 2006). The coefficients of the first fundamental form of a surface yield information about some geometric properties, which are called intrinsic geometric properties including angles of tangent vectors, the lengths of curves, the areas of regions, and so on. The second fundamental coefficients reflect the local warping of the surface, namely, its deviation from the tangent plane at the point under consideration (Liseikin 2004; Toponogov 2006). In terms of the theorem of surfaces, the first and second fundamental coefficients must satisfy the Gauss equations for uniquely defining a surface (Somasundaram 2005). The main task of HASM is to solve these Gauss equations.

The basic equations of HASM can be formulated as (Yue et al. 2007),

$$\begin{cases} f_{xx} = \Gamma_{11}^1 f_x + \Gamma_{11}^2 f_y + \dfrac{L}{\sqrt{E+G-1}} \\ f_{yy} = \Gamma_{22}^1 f_x + \Gamma_{22}^2 f_y + \dfrac{N}{\sqrt{E+G-1}} \end{cases}, \tag{1}$$

where, f_x, f_y, f_{xx}, f_{yy} represent the first and second derivatives of the function $f(x, y)$ in the x and y directions, respectively. These derivatives will be replaced with finite difference approximations on a discretized domain by using Taylor expansions to change the differential equations into finite difference equations (Yue 2011).

$$E = 1 + f_x^2,\ F = f_x \cdot f_y,\ G = 1 + f_y^2,\ L = \frac{f_{xx}}{\sqrt{1 + f_x^2 + f_y^2}},\ N = \frac{f_{yy}}{\sqrt{1 + f_x^2 + f_y^2}},$$
$$\Gamma_{11}^1 = \frac{1}{2}\left(GE_x - 2FF_x + FE_y\right)\left(EG - F^2\right)^{-1},\ \Gamma_{11}^2 = \frac{1}{2}\left(2EF_x - EE_y - FE_x\right)\left(EG - F^2\right)^{-1},$$
$$\Gamma_{22}^1 = \frac{1}{2}\left(2GF_y - GG_x - FG_y\right)\left(EG - F^2\right)^{-1},\ \Gamma_{22}^2 = \frac{1}{2}\left(EG_y - 2FF_y + FG_x\right)\left(EG - F^2\right)^{-1},$$

E, F, G are the first fundamental coefficients of the surface and represent its local details, while L, M, N are the second fundamental coefficients of the surface and denote the macroscopical information such as the shape. The Christoffel symbols ${\Gamma_{11}}^1, {\Gamma_{11}}^2, {\Gamma_{22}}^1, {\Gamma_{22}}^2$ depend only on the first fundamental coefficients and their derivatives (Somasundaram 2005).

Let $\{(x_i, y_j) | 0 \le i \le I+1, 0 \le j \le J+1\}$ be the computational grids and h be the grid size in x and y directions. Finite difference methods are used for solving equation set 1. The discrete forms of f_x, f_{xx} and f_{yy} are as follows,

$$(f_x)_{(i,j)} \approx \begin{cases} \dfrac{f_{1,j} - f_{0,j}}{h} & i = 0 \\ \dfrac{f_{i+1,j} - f_{i-1,j}}{2h} & i = 1, \ldots, I, \\ \dfrac{f_{I+1,j} - f_{I,j}}{h} & i = I+1 \end{cases} \quad (f_{xx})_{(i,j)} \approx \begin{cases} \dfrac{f_{0,j} - 2f_{1,j} + f_{2,j}}{h^2} & i = 0 \\ \dfrac{f_{i-1,j} - 2f_{i,j} + f_{i+1,j}}{h^2} & i = 1, \ldots, I \\ \dfrac{f_{I+1,j} - 2f_{I,j} + f_{I-1,j}}{h^2} & i = I+1 \end{cases}$$

$$\left(f_y\right)_{(i,j)} \approx \begin{cases} \dfrac{f_{i,1} - f_{i,0}}{h} & j = 0 \\ \dfrac{f_{i,j+1} - f_{i,j-1}}{2h} & j = 1, \ldots, J, \\ \dfrac{f_{i,J+1} - f_{i,J}}{h} & j = J+1 \end{cases} \quad \left(f_{yy}\right)_{(i,j)} \approx \begin{cases} \dfrac{f_{i,0} - 2f_{i,1} + f_{i,2}}{h^2} & j = 0 \\ \dfrac{f_{i,j-1} - 2f_{i,j} + f_{i,j+1}}{h^2} & j = 1, \ldots, J \\ \dfrac{f_{i,J+1} - 2f_{i,J} + f_{i,J-1}}{h^2} & j = J+1 \end{cases}$$

Correspondingly, Eq. 1 can be approximated by

$$\begin{cases} \dfrac{f^{n+1}_{i+1,j}-2f^{n+1}_{i,j}+f^{n+1}_{i-1,j}}{h^2} = \left(\Gamma^1_{11}\right)^n_{i,j}\dfrac{f^n_{i+1,j}-f^n_{i-1,j}}{2h} + \left(\Gamma^2_{11}\right)^n_{i,j}\dfrac{f^n_{i,j+1}-f^n_{i,j-1}}{2h} + \dfrac{L^n_{i,j}}{\sqrt{E^n_{i,j}+G^n_{i,j}-1}} \\ \dfrac{f^{n+1}_{i,j+1}-2f^{n+1}_{i,j}+f^{n+1}_{i,j-1}}{h^2} = \left(\Gamma^1_{22}\right)^n_{i,j}\dfrac{f^n_{i+1,j}-f^n_{i-1,j}}{2h} + \left(\Gamma^2_{22}\right)^n_{i,j}\dfrac{f^n_{i,j+1}-f^n_{i,j-1}}{2h} + \dfrac{N^n_{i,j}}{\sqrt{E^n_{i,j}+G^n_{i,j}-1}} \end{cases} \tag{2}$$

where n represents the number of iterations,

$$E^n_{i,j} = 1+\left(\frac{f^n_{i+1,j}-f^n_{i-1,j}}{2h}\right)^2,\ F^n_{i,j} = \left(\frac{f^n_{i+1,j}-f^n_{i-1,j}}{2h}\right)\left(\frac{f^n_{i,j+1}-f^n_{i,j-1}}{2h}\right),\ G^n_{i,j} = 1+\left(\frac{f^n_{i,j+1}-f^n_{i,j-1}}{2h}\right)^2,$$

$$L^n_{i,j} = \frac{\frac{f^n_{i-1,j}-2f^n_{i,j}+f^n_{i+1,j}}{h^2}}{\sqrt{1+\left(\frac{f^n_{i+1,j}-f^n_{i-1,j}}{2h}\right)^2+\left(\frac{f^n_{i,j+1}-f^n_{i,j-1}}{2h}\right)^2}},\quad N^n_{i,j} = \frac{\frac{f^n_{i,j-1}-2f^n_{i,j}+f^n_{i,j+1}}{h^2}}{\sqrt{1+\left(\frac{f^n_{i+1,j}-f^n_{i-1,j}}{2h}\right)^2+\left(\frac{f^n_{i,j+1}-f^n_{i,j-1}}{2h}\right)^2}},$$

$$\left(\Gamma^1_{11}\right)^n_{i,j} = \frac{G^n_{i,j}\left(E^n_{i+1,j}-E^n_{i-1,j}\right)-2F^n_{i,j}\left(F^n_{i+1,j}-F^n_{i-1,j}\right)+F^n_{i,j}\left(E^n_{i,j+1}-E^n_{i,j-1}\right)}{4\left(E^n_{i,j}G^n_{i,j}-\left(F^n_{i,j}\right)^2\right)h},$$

$$\left(\Gamma^2_{11}\right)^n_{i,j} = \frac{2E^n_{i,j}\left(F^n_{i+1,j}-F^n_{i-1,j}\right)-E^n_{i,j}\left(E^n_{i,j+1}-E^n_{i,j-1}\right)-F^n_{i,j}\left(E^n_{i,j+1}-E^n_{i,j-1}\right)}{4\left(E^n_{i,j}G^n_{i,j}-\left(F^n_{i,j}\right)^2\right)h},$$

$$\left(\Gamma^1_{22}\right)^n_{i,j} = \frac{2G^n_{i,j}\left(F^n_{i,j+1}-F^n_{i,j-1}\right)-G^n_{i,j}\left(G^n_{i+1,j}-G^n_{i-1,j}\right)-F^n_{i,j}\left(G^n_{i,j+1}-G^n_{i,j-1}\right)}{4\left(E^n_{i,j}G^n_{i,j}-\left(F^n_{i,j}\right)^2\right)h},$$

$$\left(\Gamma^2_{22}\right)^n_{i,j} = \frac{E^n_{i,j}\left(G^n_{i,j+1}-G^n_{i,j-1}\right)-2F^n_{i,j}\left(F^n_{i,j+1}-F^n_{i,j-1}\right)+F^n_{i,j}\left(G^n_{i+1,j}-G^n_{i-1,j}\right)}{4\left(E^n_{i,j}G^n_{i,j}-\left(F^n_{i,j}\right)^2\right)h}.$$

The matrix formulation of Eq. 2 can be expressed as

$$\begin{cases} \mathbf{A}x^{n+1} = d^n \\ \mathbf{B}x^{n+1} = q^n \end{cases} \tag{3}$$

where $x^{n+1}=(f^{n+1}_{1,1},\ldots,f^{n+1}_{1,J},f^{n+1}_{2,1},\ldots,f^{n+1}_{2,J},\ldots,f^{n+1}_{I-1,1},\ldots,f^{n+1}_{I-1,J},f^{n+1}_{I,1},\ldots,f^{n+1}_{I,J})^T$.

$$A = \begin{bmatrix} -2I & I & & & \\ I & -2I & I & & \\ & \ddots & \ddots & \ddots & \\ & & I & -2I & I \\ & & & I & -2I \end{bmatrix}_{I\cdot J\times I\cdot J},\quad I = \begin{bmatrix} 1 & & \\ & \ddots & \\ & & 1 \end{bmatrix}_{J\times J},$$

$$B = \begin{bmatrix} \widehat{B} & & \\ & \ddots & \\ & & \widehat{B} \end{bmatrix}_{I\cdot J\times I\cdot J},\qquad \widehat{B} = \begin{bmatrix} -2 & 1 & & & & & \\ 1 & -2 & 1 & & & & \\ & \ddots & \ddots & \ddots & & & \\ & & 1 & -2 & 1 & & \\ & & & \ddots & \ddots & \ddots & \\ & & & & 1 & -2 & 1 \\ & & & & & 1 & -2 \end{bmatrix}_{J\times J},$$

A and **B** denote the coefficient matrices of Eq. 3 and ***d***, ***q*** are the right-hand vectors, respectively. The boundary values of HASM are obtained using other interpolators, such as kriging, and are not yet changed during iterations.

The following equality-constrained least squares problem is developed to make the interpolated values equal to or approximate to the sampled values at the sampling points,

$$\begin{cases} \min\left\| \begin{bmatrix} A \\ B \end{bmatrix} x^{n+1} - \begin{bmatrix} d \\ q \end{bmatrix}^n \right\|_2 \\ Sx^{n+1} = k \end{cases} \tag{4}$$

where $S(l,\ (i-1)\cdot J+j)=1,\ k(l)=\overline{f}_{i,j}$, this means that the value of the lth sampling point (x_i,y_j) is $\overline{f}_{i,j}$. However, when the sampling point deviates from the grid point, we should

find out the nearest grid point for which Taylor expansion is used to give an approximate value of this point.

An interesting way to obtain an approximate solution to Eq. 4 is to solve the unconstrained least squares problem,

$$\min_x \left\| \begin{bmatrix} A \\ B \\ \lambda S \end{bmatrix} x^{n+1} - \begin{bmatrix} d \\ q \\ \lambda k \end{bmatrix}^n \right\|_2 \tag{5}$$

for large λ (Golub and Van Loan 2009). This problem is equivalent to the symmetric positive definite linear system,

$$\mathbf{W}x^{n+1} = v^n \tag{6}$$

where $\mathbf{W}=A^{\mathrm{T}}A+B^{\mathrm{T}}B+\lambda S^{\mathrm{T}}S$ reflects the local relationship of the surrounding points since $\mathbf{W}$ is a sparse matrix of which the nonzero elements in each row denote the coefficients of the relationship between each point and the surrounding points. $v^n=A^{\mathrm{T}}d^n+B^{\mathrm{T}}q^n+\lambda^2 S^{\mathrm{T}}k^n$ is the right-hand vector; λ is the weight of the sampling points. For large values of λ, however, numerical problems arise (Golub and Van Loan 2009). Therefore, for a specific application, we must adjust this parameter until a reasonable agreement is attained between model output and field measurement. $\boldsymbol{x}$ is a vector that each element denotes the simulated value of the corresponding grid point.

3.2 A modified version of HASM

Since mathematical methods cannot explain all the variability due to the climate anomalies, it seems that the optimal situation to produce accurate precipitation surface is to begin with an objective method that could be revised by experts. A recent review about the combination of expert knowledge and mathematical tools applied to climate mapping can be found in the report of Daly et al. (2002). However, the method is based on a linear regression function between climate and elevation, which is difficult to satisfy in practical applications especially in China. Brus and Heuvelink (2007) stated that, besides the data type, area of interest and computation capacity, the quality of the spatial prediction was also subject to the spatial patterns of the observations. In this section, we modify HASM by taking into account the phenomenon of the spatial distribution of precipitation.

Note that although HASM is based on the fundamental theorem of surface, the theoretical basis of it is not complete, without considering the mixed derivatives $f_{xy}=\Gamma^1_{12}f_x+\Gamma^2_{12}f_y+\frac{M}{\sqrt{E+G-1}}$ of the equations of surface theory (Yue 2011). Since f_{xy} reflects the local warping of the surface, namely, its deviation from tangent plane at the point under consideration (Liseikin 2004), we then add this equation into HASM to make it theoretically perfect. In addition, we propose a specific discrete scheme of f_{xy} according to the spatial distribution pattern of precipitation in China.

Consider the following partial differential equations of the surface theory, namely, Gauss equations (Somasundaram 2005),

$$\begin{cases} f_{xx} = \Gamma^1_{11}f_x + \Gamma^2_{11}f_y + \dfrac{L}{\sqrt{E+G-1}} \\ f_{yy} = \Gamma^1_{22}f_x + \Gamma^2_{22}f_y + \dfrac{N}{\sqrt{E+G-1}} \\ f_{xy} = \Gamma^1_{12}f_x + \Gamma^2_{12}f_y + \dfrac{M}{\sqrt{E+G-1}} \end{cases}, \tag{7}$$

where the first two equations are the main predictive equations of HASM. In the third equation,

$$M = \frac{f_{xy}}{\sqrt{1+f_x^2+f_y^2}}, \Gamma^1_{12} = \frac{1}{2}\left(GE_y - FG_x\right)\left(EG-F^2\right)^{-1},$$
$$\Gamma^2_{12} = \frac{1}{2}\left(EG_x - FE_y\right)\left(EG-F^2\right)^{-1}.$$

The discrete forms of f_x, f_y, f_{xx} and f_{yy} are the same as in HASM. Since the precipitation shows a strong southeast–northwest trend, we can use the neighboring observations located in the southeast and northwest to predict attributed values at unsampled locations (i, j). Therefore, by employing Taylor expansion, $f_{i+1,j-1}, f_{i+1,j}, f_{i,j-1}$ located in the northwest and $f_{i-1,j+1}, f_{i,j+1}, f_{i-1,j}$ from the southeast can be formulated as the following Taylor expansions in series

$$f_{i+1,j-1} = f_{i,j} + hf_x - hf_y + \frac{h^2}{2}f_{xx} + \frac{h^2}{2}f_{yy} - h^2 f_{xy} + O\left(h^2\right), \tag{8}$$

$$f_{i+1,j} = f_{i,j} + hf_x + \frac{h^2}{2}f_{xx} + O\left(h^2\right), \tag{9}$$

$$f_{i,j-1} = f_{i,j} - hf_y + \frac{h^2}{2}f_{yy} + O\left(h^2\right), \tag{10}$$

$$f_{i-1,j+1} = f_{i,j} - hf_x + hf_y + \frac{h^2}{2}f_{xx} + \frac{h^2}{2}f_{yy} - h^2 f_{xy} + O\left(h^2\right), \tag{11}$$

$$f_{i,j+1} = f_{i,j} + hf_y + \frac{h^2}{2}f_{yy} + O\left(h^2\right), \tag{12}$$

$$f_{i-1,j} = f_{i,j} - h f_x + \frac{h^2}{2} f_{xx} + O(h^2). \tag{13}$$

Hence, for the inner points of the computational grid, we have

$$f_{xy} \approx \frac{1}{2h^2}\left(f_{i+1,j} + f_{i,j-1} + f_{i,j+1} + f_{i-1,j} - f_{i+1,j-1} - f_{i-1,j+1} - 2f_{i,j}\right).$$

The formulation of the boundary point can be obtained in the same way. Then, the discrete forms of f_{xy} are as follows:

$$\left(f_{xy}\right)_{(i,j)} \approx \begin{cases} \dfrac{f_{1,1} - f_{1,0} - f_{0,1} + f_{0,0}}{h^2} & i = 0, j = 0 \\ \dfrac{f_{1,J+1} - f_{1,J} - f_{0,J+1} + f_{0,J}}{h^2} & i = 0, j = J+1 \\ \dfrac{f_{1,j+1} - f_{0,j+1} - f_{1,j-1} + f_{0,j-1}}{2h^2} & i = 0, j = 1, \cdots, J \\ \dfrac{f_{I+1,1} - f_{I,0} - f_{I,1} + f_{I+1,0}}{h^2} & i = I+1, j = 0 \\ \dfrac{f_{I,J} - f_{I+1,J} - f_{I,J+1} + f_{I+1,J+1}}{h^2} & i = I+1, j = J+1 \\ \dfrac{f_{I+1,j+1} - f_{I,j+1} - f_{I+1,j-1} + f_{I,j-1}}{2h^2} & i = I+1, j = 1, \ldots, J \\ \dfrac{f_{i+1,1} - f_{i+1,0} - f_{i-1,1} + f_{i-1,0}}{2h^2} & i = 1, \ldots, I, j = 0 \\ \dfrac{f_{i+1,J+1} - f_{i+1,J} - f_{i-1,J+1} + f_{i-1,J}}{2h^2} & i = 1, \ldots, I, j = J+1 \\ \dfrac{f_{i+1,j} - f_{i+1,j-1} - f_{i-1,j+1} - 2f_{i,j} + f_{i,j-1} + f_{i,j+1} + f_{i-1,j}}{2h^2} & i = 1, \ldots, I, j = 1, \ldots, J. \end{cases}$$

For the inner points, the distribution of the surrounding points used to represent spatial correlation is shown in Fig. 2.

Therefore, the equations of HASM-PRE are as follows:

$$\begin{cases} \dfrac{f^{n+1}_{i+1,j} - 2f^{n+1}_{i,j} + f^{n+1}_{i-1,j}}{h^2} = \left(\Gamma^1_{11}\right)^n_{i,j} \dfrac{f^n_{i+1,j} - f^n_{i-1,j}}{2h} + \left(\Gamma^2_{11}\right)^n_{i,j} \dfrac{f^n_{i,j+1} - f^n_{i,j-1}}{2h} + \dfrac{L^n_{i,j}}{\sqrt{E^n_{i,j} + G^n_{i,j} - 1}} \\ \dfrac{f^{n+1}_{i,j+1} - 2f^{n+1}_{i,j} + f^{n+1}_{i,j-1}}{h^2} = \left(\Gamma^1_{22}\right)^n_{i,j} \dfrac{f^n_{i+1,j} - f^n_{i-1,j}}{2h} + \left(\Gamma^2_{22}\right)^n_{i,j} \dfrac{f^n_{i,j+1} - f^n_{i,j-1}}{2h} + \dfrac{N^n_{i,j}}{\sqrt{E^n_{i,j} + G^n_{i,j} - 1}} \\ \dfrac{f^{n+1}_{i+1,j} - f^{n+1}_{i+1,j-1} - f^{n+1}_{i-1,j+1} - 2f^{n+1}_{i,j} + f^{n+1}_{i,j-1} + f^{n+1}_{i,j+1} + f^{n+1}_{i-1,j}}{2h^2} = \left(\Gamma^1_{12}\right)^n_{i,j} \dfrac{f^n_{i+1,j} - f^n_{i-1,j}}{2h} + \left(\Gamma^2_{12}\right)^n_{i,j} \dfrac{f^n_{i,j+1} - f^n_{i,j-1}}{2h} + \dfrac{M^n_{i,j}}{\sqrt{E^n_{i,j} + G^n_{i,j} - 1}} \end{cases} \tag{14}$$

where

$$M^n_{i,j} = \frac{\dfrac{f^n_{i+1,j} - f^n_{i+1,j-1} - f^n_{i-1,j+1} - 2f^n_{i,j} + f^n_{i,j-1} + f^n_{i,j+1} + f^n_{i-1,j}}{2h^2}}{\sqrt{1 + \left(\frac{f^n_{i+1,j} - f^n_{i-1,j}}{2h}\right)^2 + \left(\frac{f^n_{i,j+1} - f^n_{i,j-1}}{2h}\right)^2}},$$

$$\left(\Gamma^1_{12}\right)^n_{i,j} = \frac{G^n_{i,j}\left(E^n_{i+1,j} - E^n_{i-1,j}\right) - F^n_{i,j}\left(G^n_{i+1,j} - G^n_{i-1,j}\right)}{4\left(E^n_{i,j} G^n_{i,j} - \left(F^n_{i,j}\right)^2\right)h},$$

$$\left(\Gamma^2_{12}\right)^n_{i,j} = \frac{E^n_{i,j}\left(G^n_{i+1,j} - G^n_{i-1,j}\right) - F^n_{i,j}\left(E^n_{i,j+1} - E^n_{i,j-1}\right)}{4\left(E^n_{i,j} G^n_{i,j} - \left(F^n_{i,j}\right)^2\right)h}.$$

Like the form of HASM, the constraint equation about sample point information is added to Eq. 14, and the formulation of HASM-PRE can be expressed as

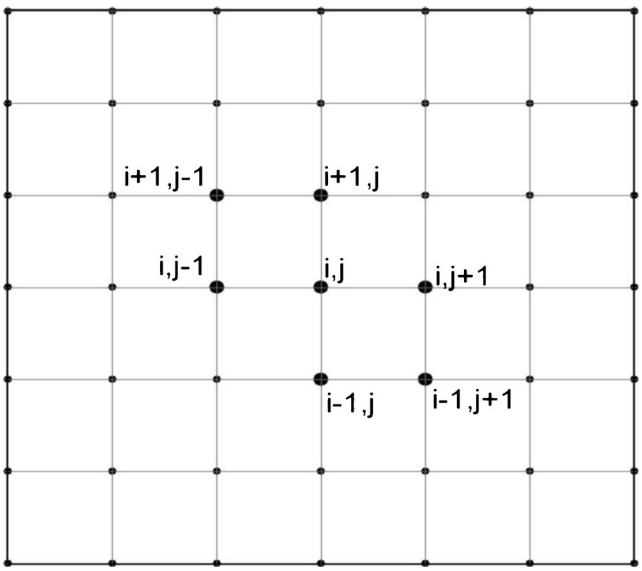

Fig. 2 Stencil for differentiation of the mixed derivative f_{xy}

$$\begin{cases} \min \left\| \begin{bmatrix} A \\ B \\ C \end{bmatrix} z^{n+1} - \begin{bmatrix} d \\ q \\ p \end{bmatrix}^n \right\|_2 \\ \text{s.t.} Sz^{(n+1)} = k \end{cases} \tag{15}$$

where

$$A = \begin{bmatrix} -2I & I & & & \\ I & -2I & I & & \\ & \ddots & \ddots & \ddots & \\ & & I & -2I & I \\ & & & I & -2I \end{bmatrix}_{(I+2)\cdot(J+2)\times(I+2)\cdot(J+2),} \quad I = \begin{bmatrix} 1 & & \\ & \ddots & \\ & & 1 \end{bmatrix}_{(J+2)\times(J+2)}$$

$$B = \begin{bmatrix} \widetilde{B} & & \\ & \ddots & \\ & & \widetilde{B} \end{bmatrix}_{(I+2)\cdot(J+2)\times(I+2)\cdot(J+2),} \quad \widetilde{B} = \begin{bmatrix} -2 & 1 & & & & & \\ 1 & -2 & 1 & & & & \\ & \ddots & \ddots & \ddots & & & \\ & & 1 & -2 & 1 & & \\ & & & \ddots & \ddots & \ddots & \\ & & & & 1 & -2 & 1 \\ & & & & & 1 & -2 \end{bmatrix}_{(J+2)\times(J+2)}$$

$$C = \begin{bmatrix} C_1 & -C_1 & & & \\ C_3 & C_2 & C_4 & & \\ & \ddots & \ddots & \ddots & \\ & & C_3 & C_2 & C_4 \\ & & & C_1 & -C_1 \end{bmatrix}_{(I+2)\cdot(J+2)\times(I+2)\cdot(J+2),} \quad C_1 = \begin{bmatrix} 1 & -1 & & & \\ 1/2 & 0 & -1/2 & & \\ & \ddots & \ddots & \ddots & \\ & & 1/2 & 0 & -1/2 \\ & & & 1 & -1 \end{bmatrix}_{(J+2)\times(J+2)}$$

$$C_2 = \begin{bmatrix} 0 & 0 & 0 & & \\ 1/2 & -1 & 1/2 & & \\ & \ddots & \ddots & \ddots & \\ & & 1/2 & -1 & 1/2 \\ & & 0 & 0 & 0 \end{bmatrix}_{(J+2)\times(J+2),} \quad C_3 = \begin{bmatrix} 1/2 & -1/2 & & & \\ & 1/2 & -1/2 & & \\ & & \ddots & \ddots & \\ & & & 1/2 & -1/2 \\ & & & 1/2 & -1/2 \end{bmatrix}_{(J+2)\times(J+2)}$$

$$C_4 = \begin{bmatrix} -1/2 & 1/2 & & & \\ -1/2 & 1/2 & & & \\ & \ddots & \ddots & & \\ & & -1/2 & 1/2 & \\ & & & -1/2 & 1/2 \end{bmatrix}_{(J+2)\times(J+2).}$$

A, B, C are the left-hand sides of Eq. 14, respectively. For the inner grid points, A and B are identical to those in HASM.

By introducing a Lagrange parameter λ, we finally get the matrix equation of HASM-PRE,

$$\overline{A}x^{n+1} = \overline{b}^n \tag{16}$$

Table 1 Means and standard deviations of RMSEs and MAEs of 20 validation sets for HASM-PRE, HASM, kriging, IDW and spline

Methods	HASM-PRE	HASM	Kriging	IDW	Spline
RMSE (mm)	91.04	132.84	131.33	145.76	135.44
$RMSE_{STD}$ (mm)	18.31	24.74	23.37	25.08	33.83
MAE (mm)	52.87	91.06	77.51	88.22	81.33
MAE_{STD} (mm)	12.76	14.16	13.05	16.83	17.00

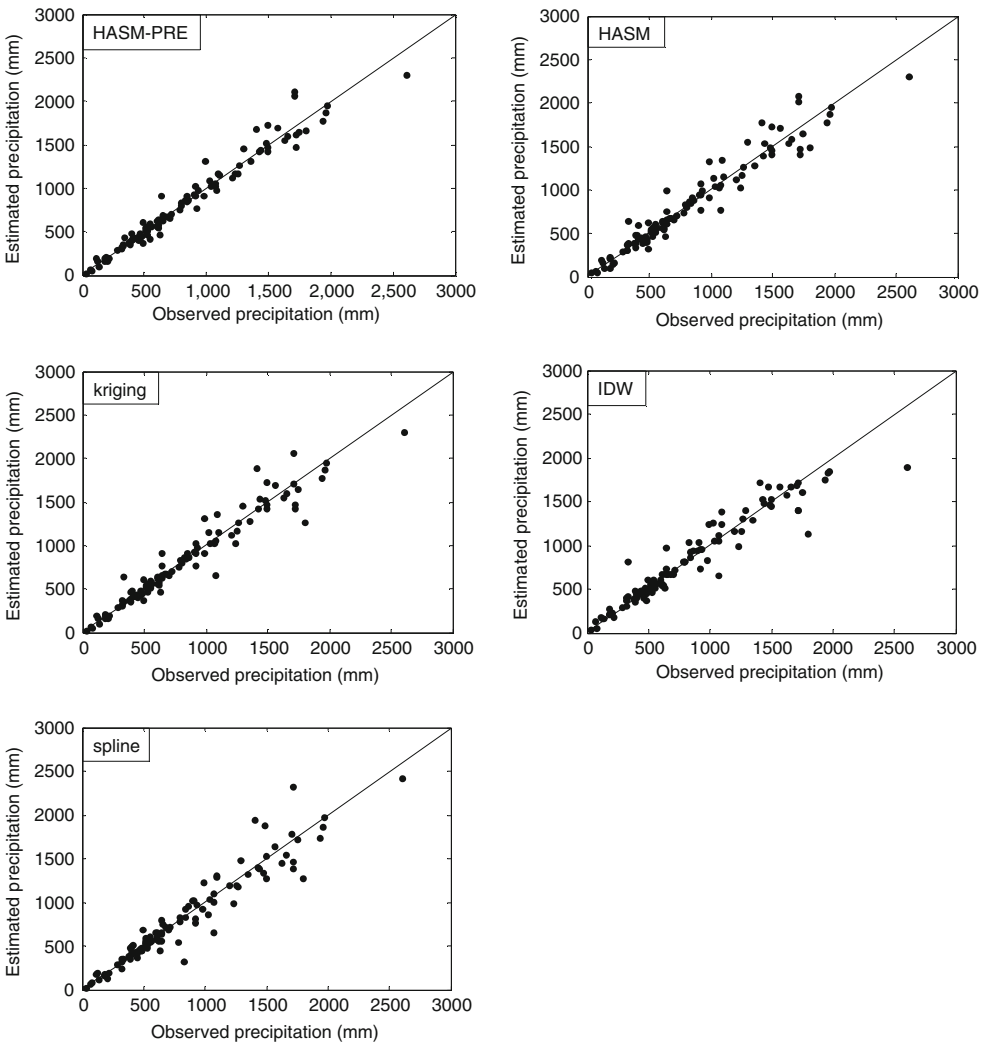

Fig. 3 Observed and estimated precipitation using different models

where

$$\overline{A} = A^{\mathrm{T}}A + B^{\mathrm{T}}B + C^{\mathrm{T}}C + \lambda^2 S^{\mathrm{T}}S \quad \text{and} \quad \overline{b} = A^{\mathrm{T}}d + B^{\mathrm{T}}q + C^{\mathrm{T}}p + \lambda^2 S^{\mathrm{T}}\dot{k}.$$

4 Results and analyses

4.1 Comparison of interpolation performance

A total of 107 stations were selected at random from the data set and withheld from the interpolation calculations. This process was repeated 20 times. Two indices, root mean square error (RMSE) and mean absolute error (MAE), were calculated from the station value and interpolated value at each validation sample site. The formulations of RMSE and MAE are:

$$\mathrm{RMSE} = \sqrt{\frac{1}{N}\sum_{k=1,\ldots,N}\left(f_k - \overline{f}_k\right)^2}, \quad \mathrm{MAE} = \frac{1}{N}\sum_{k=1,\ldots,N}\left|f_k - \overline{f}_k\right|$$

where f_k is the true value at the kth point (x_i, y_j); $\overline{f}_k$ is the simulated value; N is the number of validation points. The values of these criteria should be close to zero if the method is accurate. In comparison, RMSE is sensitive to the size of outliers and is used as an indicator of the magnitude of extreme errors. Lower RMSE indicates greater central tendency and generally smaller extreme error (Vicente-Serrano et al. 2003).

We compared the performance of HASM-PRE, HASM and those of ordinary kriging (OK), IDW, and spline methods. These classical methods were performed using the module of 3D analyst ArcGIS 10.1. Different parameters for OK, IDW and spline were compared, and the best parameters for each technique with the smallest RMSE values were decided. For OK, the exponential, spherical, Gaussian and linear models were fitted to the experimental variogram and the number of the closest samples chosen varied from 5 to 30. IDW was estimated with powers of 1, 2, 3 and 4. For spline, the regularized and tension methods were implemented using the same neighborhood variations as those used in OK and IDW.

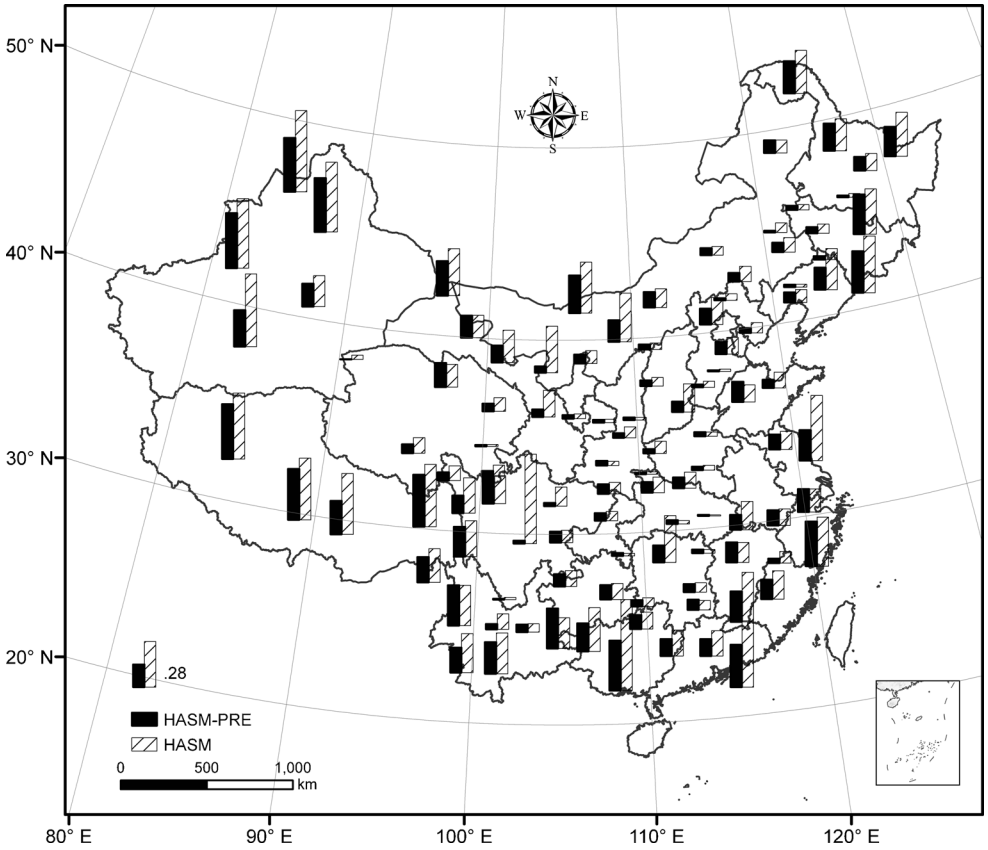

Fig. 4 Relative errors produced by HASM-PRE and HASM at each verification point

Table 1 compares the means and standard deviations of 20 RMSEs and MAEs obtained using the five interpolators. $RMSE_{STD}$ and MAE_{STD} mean the standard deviations of 20 RMSEs and MAEs, respectively. Those obtained using HASM-PRE are lower than those of other methods. The results of HASM, kriging, IDW and spline show small differences. HASM is the least exact of the five based on MAE values. The largest RMSE value is obtained by IDW and smoothing routines of HASM-PRE, HASM, kriging and spline result in lower RMSEs. The smallest RMSE value is produced by HASM-PRE since the consideration of mixed derivative f_{xy} which makes the simulation surface smoother (Malik and Savita 1992). The standard deviations of RMSEs and MAEs also indicate the best performance of HASM-PRE, which is followed by kriging method.

Scatter correlation plots for the observed and predicted precipitation (Fig. 3) suggest that HASM-PRE estimates the annual mean precipitation quite reliably. Many simulation points are relatively far from the straight line of $y = x$ by using other methods including HASM. Overestimation of precipitation is obvious for HASM-PRE, HASM and kriging. Under- and overestimation of precipitation are evident from IDW and spline. The correlation coefficient between predicted and observed values is 0.99 for HASM-PRE and 0.97 for HASM. The correlation coefficients are 0.97, 0.96 and 0.96 for kriging, IDW and spline, respectively.

In order to make a better comparison between HASM-PRE and HASM, Fig. 4 displays the difference between the simulated value and observed value at each validation point produced by both methods. It is evident that large errors usually occur in rough mountain areas, western China and the border of China, for both methods. However, in the inland regions of China, the absolute values of relative errors produced by HASM-PRE are much smaller than those by HASM at most of the locations. This is possibly because of the lack of mixed partial derivative of the surface, which reflects the local warping of the surface, and then the particular discrete form of f_{xy}. The feature of HASM-PRE is that it performs better in the inland areas of China than in its borders, possibly due to the lack of sample information outside the boundary, which means that there is no difference schemes to characterize the distribution patterns of precipitation for f_{xy} at the point (i, j) near the Chinese border. The performance of HASM displays no clear pattern. Large errors can be seen both in internal points and boundary points for HASM. This is possibly because of the undefined discrete schemes of HASM with respect to the physical variables of precipitation.

Besides the bad performance near the border, the predictions of HASM-PRE and HASM are relatively poor in the regions of complex topography, such as in Hengduan mountains (Fig. 4). Large precipitation totals are mostly caused by orogaphical lifting of the air masses which thus yield a large

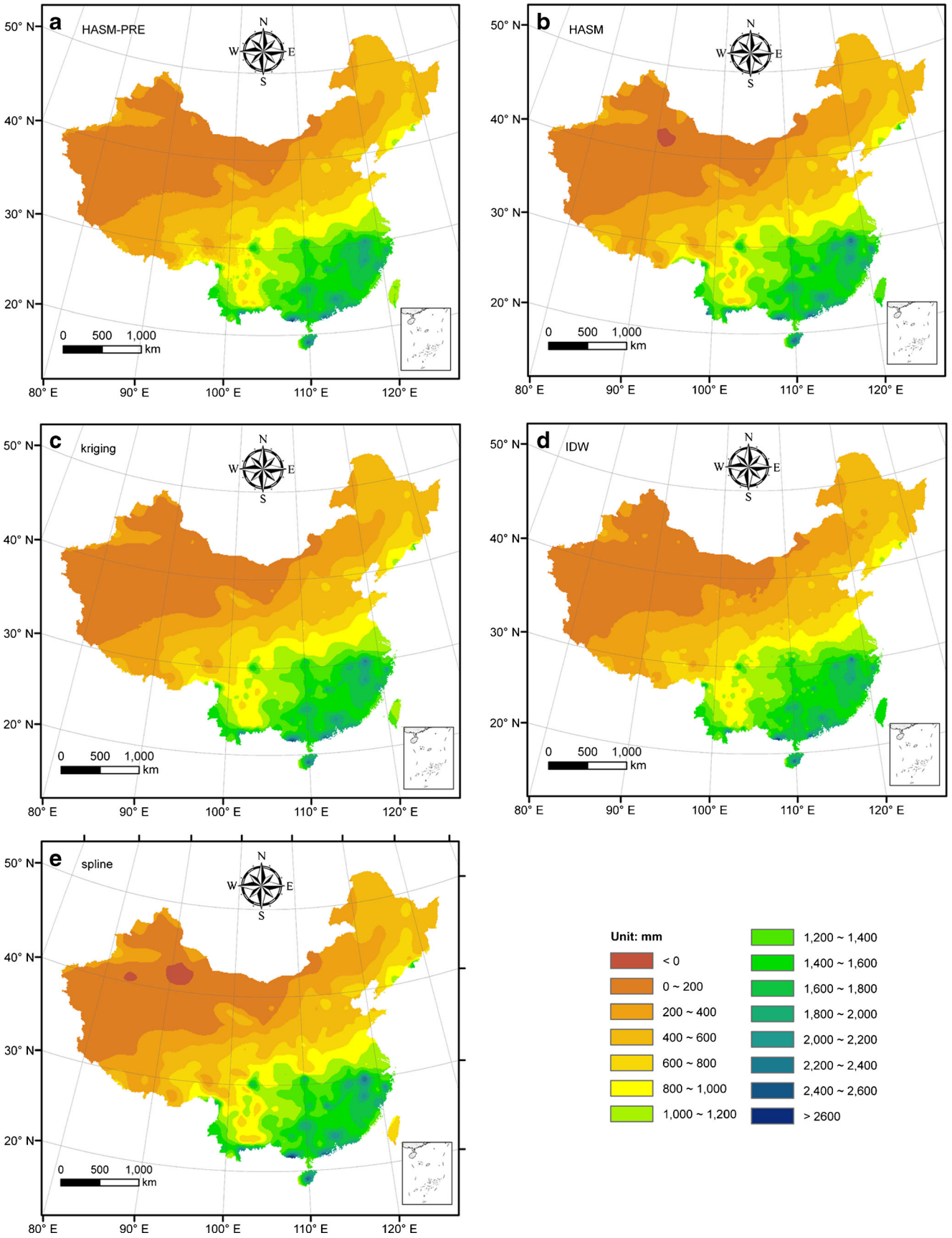

Fig. 5 Predicted mean annual precipitation over the period 1951–2010 using: **a** HASM-PRE, **b** HASM, **c** kriging, **d** IDW, **e** spline

Table 2 Errors for annual mean precipitation generated by HASM-PRE and HASM.MOD

Methods	HASM-PRE	HASM.MOD
RMSE (mm)	91.04	131.74
MAE (mm)	52.87	89.58

amount of orographical precipitation on the wind-exposed slopes. The performance of HASM-PRE and HASM is worse near the high mountains of inner China since both methods have not considered the considerably varying landforms. Several studies show that the accuracy of interpolations could be improved if the effect of many geographical and topographical factors on climate parameters are considered in the interpolation process (Ninyerola et al. 2000; Marquinez et al. 2003; Portales et al. 2010; Aalto et al. 2012; Samanta et al. 2012). It seems worthwhile to account for this exhaustive secondary information into the mapping of precipitation especially in rough terrain areas, such as in China.

4.2 Comparison of the interpolated maps by the five techniques

The patterns of precipitation distribution produced by different interpolators using 712 points are displayed in Fig. 5. All simulation surfaces show the increasing precipitation pattern from northwest to southeast over China. Spline has a serious oscillation problem which makes the minimum output (−59.88 mm) lower and the maximum output (2,734.40 mm) higher than those of other techniques (Fig. 5e). Moreover, spline predicts negative precipitation especially in data-sparse regions which does not agree with the actual situations. IDW interpolation produces many "bull's eyes," which means that we can see higher or lower values near observed locations (Fig. 5d). This phenomenon is possibly due to the fewer points used in IDW. If we use more points in the vicinity of the outliers, we can expect a smoother result. In addition, we find there are some obvious outliers in the southern and eastern China for all methods, which make this phenomenon even more pronounced. We find that these stations are located in the mountainous areas. The precipitation amount in these places is higher than in the surrounding areas possibly because of the Foehn effect. The smoother surfaces can be obtained by HASM-PRE, HASM and kriging. However, negative precipitation is produced by HASM as is shown in Fig. 5b, and the kriging method does not show significantly greater predictive capability than HASM-PRE, as illustrated in Table 1.

4.3 The main reason for the improved accuracy of HASM-PRE

HASM-PRE takes into account the third equation in Gauss equations and uses the particular discrete form of f_{xy}. We have shown that the performance of HASM-PRE is better than HASM and other classical methods when interpolating the annual precipitation in China. We then explore the main reason for the improvement in accuracy of HASM-PRE by comparing different discrete schemes of f_{xy}.

For the inner grid points, the classic discrete scheme of f_{xy} is as follows:

$$\left(f_{xy}\right)_{(i,j)} \approx \frac{f_{i+1,j+1} - f_{i-1,j+1} + f_{i-1,j-1} - f_{i+1,j-1}}{4h^2}, \quad i = 1, \ldots, I, j = 1, \ldots, J,$$

which uses the points distributed in the surrounding of the point (x_i, y_j). However, this discrete form of f_{xy} leads to algebraic systems with loss of diagonal dominance and thus computational complexity, which eventually leads to a stack overflow in HASM simulation (Yue 2011).

Since f_{xy} can be also expressed by using neighboring observations located in the southeast–northwest or the southwest–northeast direction, we then check the performance of HASM based on these two different discrete forms of f_{xy}. For the southwest–northeast direction, the discrete scheme of f_{xy} is

$$\left(f_{xy}\right)_{(i,j)} \approx \frac{f_{i+1,j+1} - f_{i+1,j} - f_{i,j+1} + 2f_{i,j} - f_{i-1,j} - f_{i,j-1} + f_{i-1,j-1}}{2h^2} \quad (17)$$
$$i = 1, \ldots, I, \; j = 1, \ldots, J.$$

The results are shown in Table 2. HASM.MOD denotes that we use the three equations of Gauss equations and employ the discrete forms of f_{xy} as is shown in Eq. 17. Combined with the results in Table 1, HASM.MOD performs slightly better than HASM but worse than HASM-PRE. It can be concluded that the improvement of the simulation accuracy is not significant by introducing the third equation in Gauss equations. Compared with the introduction of the third equation, the special discrete scheme of f_{xy} based on the distribution characteristic of precipitation has a greater effect on the simulation accuracy.

5 Discussion

We calculated RMSEs and MAEs to compare the accuracy of HASM-PRE, HASM and other interpolators — kriging, IDW, spline — which demonstrated the highest accuracy of HASM-PRE. Scatter plots and precipitation distribution surfaces were also displayed to show the superiority of HASM-PRE over other spatial interpolation methods. Kriging results rely heavily on a previously well-chosen semivariogram, which is difficult to estimate and validate against a true covariance function. Moreover, kriging method generally assumes normally distributed variables, which is a difficult condition to satisfy in practical applications (Goovaerts 1999). Another frequently used model in spatial interpolation is the IDW method. There are no assumptions required of the input data for the application of IDW. However, IDW relies mainly

on the inverse of the distance raised to the power and can also be controlled by limiting the input points for calculating each interpolated point. Spline is an interpolation method that estimates values using a mathematical function that minimizes overall surface curvature, resulting in a smooth surface. However, this method tends to generate steep gradients in data-poor areas leading to compounded errors in the estimation process (Wang 2006). Compared with these popular methods, HASM avoids the subjectivity involved in defining variogram models and neighborhoods. Besides, just like IDW, there are no assumptions required of the input data and the solutions are estimated by an iterative process like spline.

Since we solve the partial differential equations of the surface in the whole studied area, HASM can be regarded as a global method in which all the available data for a given study area are used, resulting in a smooth surface. In fact, smoothness is inherent to HASM because the partial derivatives of the simulated surface f are supposed to exist. Meanwhile, HASM can be treated as a local method as it capitalizes on the spatial correlation between neighboring observations by using Taylor expansion. Consequently, local anomalies can be accommodated without affecting the value of interpolation at other points on the surface. A combination of global technique and local technique ensures that HASM is another alternative surface modeling method. However, the earlier version of HASM lacks integrity in theory, and the symbols and the discrete ways of the differential equations in HASM are unrelated with precipitation, which make HASM perform worse in interpolating precipitation.

In terms of the fundamental theorem of surface, a surface is uniquely defined by the first fundamental coefficients and the second fundamental coefficients (Henderson 1998; Toponogov 2006). The geometric properties determined by the first fundamental coefficients of a surface are called the intrinsic geometric properties, such as the lengths of curves in the surface, which do not depend on the shape of the surface. The second fundamental coefficients reflect the local warping of the surface, namely, its deviation from tangent plane at the point under consideration (Liseikin 2004). HASM ignores the second fundamental coefficient M, yet HASM-PRE is theoretically perfect, which insures that it performs best and improves HASM's simulation skills. In addition, the difference scheme for the mixed derivative f_{xy} used in this study is particularly important for accurate precipitation interpolation in China. Another different feature between HASM-PRE and HASM is that HASM-PRE considers the whole studied area while HASM ignores the boundary points. HASM-PRE is still sensitive to edge effects possibly because of its reliance on Taylor expansion. However, like other techniques, if additional stations beyond the boundary are available, we can expect a better result near the edge of China.

Distribution of precipitation is controlled by several geographical and topographical factors, like DEM, distance from the coastline, slope, orientation, and exposure (Basisr et al. 1994; Goovaerts 2000; Marquinez et al. 2003). Precipitation varies severely within a short distance, so it is difficult to interpolate accurately using HASM when we ignore such obvious factors. This is equally true with kriging, and auxiliary variables can be used in several ways, such as in cokriging and kriging with external drift (Seo 1996; Aalto et al. 2012). Similarly, HASM-PRE has the potential for increased accuracy via introduction of additional independent variables known to have effects on precipitation.

6 Conclusions

Many interpolation methods are used in climatology but all have their limits so that the quality of estimations produced varies greatly with context. In this research, based on the spatial distribution characteristics of mean annual precipitation in China, we give a modification of HASM, namely, HASM-PRE. We use the wealth of expert knowledge on the spatial patterns of precipitation to establish the discrete schemes of the partial differential equations of the surface theory. Then we validate the effectiveness of HASM-PRE by comparing it with HASM and other popular interpolators. Our study showed that the proposed technique is more accurate for predicting the spatial patterns of precipitation than other methods. The proposed method can be used for calculating precipitation for other areas in other temporal scale by taking into account the different difference schemes for the respective area.

Its disadvantage is that HASM-PRE becomes more complex as one begins to solve more complicated nonlinear system and thus requires more computing and modeling time. However, HASM-PRE can be developed further for application in the parallel environment. The parallel implementation of HASM-PRE combined with ancillary variables makes HASM-PRE more perfect.

Acknowledgments We thank the editor and the reviewers for their valuable comments, suggestions, and revisions on this manuscript. This work is supported by National Key Technologies R&D Program of the Ministry of Science and Technology of the People's Republic of China (2013BACO3B05), by National Basic Research Priorities Program of Ministry of Science and Technology of the People's Republic of China (2010CB950904), and by the Key Program of National Natural Science of China (41023010). We acknowledge Dr. Wenjiao Shi (Institute of Geographic Sciences and Natural Resources Research, CAS) for her contributions in the language revision and useful suggestions.

References

Aalto J, Pirinen P, Heikkinen J, Venalainen A (2012) Spatial interpolation of monthly climate data for Finland: comparing the performance of kriging and generalized additive models. Theor Appl Climatol 112(1–2):99–111

Basisr A, Bell GD, Meentemeyer V (1994) Statistical relationships between topography and precipitation patterns. J Climate 7(9):1305–1315
Brus D, Heuvelink G (2007) Optimization of sample patterns for universal kriging of environmental variables. Geoderma 138:86–95
Burrough PA, McDonnell RA (1998) Principles of geographical information systems. Oxford University Press, New York
Carmo MP (2006) Differential geometry of curves and surfaces. China Machine Press, Beijing
Daly C, Neilson RP, Phillips DL (1994) A statistical-topographical model for mapping climatological precipitation over mountainous terrain. J Appl Meteorol 33:140–158
Daly C, Taylor GH, Gibson WP, Parzybok TW, Johnson GL, Pasteris P (2001) High-quality spatial climate data sets for the United States and beyond. Trans Am Soc Agric Eng 43:1957–1962
Daly C, Gibson WP, Taylor GH, Johnson GL, Pasteris P (2002) A knowledge-based approach to the statistical mapping of climate. Clim Res 22:99–113
DeGaetano AT, Wilks DS (2009) Radar-guided interpolation of climatological precipitation data. Int J Climatol 29:185–196
Dingman SL, Seely-Reynolds DM, Reynolds RC III (1998) Application of kriging to estimate mean annual precipitation in a region of orographic influence. Water Resour Bull 24:29–339
Domroes M, Peng G (1988) The climate of China. Spring-Verlag, Berlin
Fronzek S, Luoto M, Carter T (2006) Potential effect of climate change on the distribution of palsa-mires in subarctic Fennoscandia. Clim Res 32:1–12
Golub GH, Van Loan CF (2009) Matrix computations. Posts & Telecom Press, Beijing
Goovaerts P (1999) Geostatistics in soil science: state-of-the-art and perspectives. Geoderma 89:1–45
Goovaerts P (2000) Geostatstical approaches for incorporating elevation into the spatial interpolation of rainfall. J Hydrol 228:113–129
Hasenauer H, Merganicova K, Petritsch R, Pietsch SA, Thomton PE (2003) Validation daily climate interpolations over complex terrain in Austria. Agric For Meteorol 119(1–2):87–107
Henderson DW (1998) Differential geometry. Prentice-Hall, London
Hevesi JA, Istok JD, Flint AL (1992) Precipitation estimation in mountainous terrain using multivariate geostatistics: 1. Structural analysis. J Appl Meteorol 31:661–676
Hijmans RJ, Cameron S, Parra JL, Jones PJ, Jarvis A (2006) Very high resolution interpolated climate surfaces for global land areas. Int J Climatol 25:1965–1978
Hutchinson MF (1995) Interpolating mean rainfall using thin plate smoothing spline. Int J Gis 9:385–403
Kullmann L (2010) A richer, greener and smaller alpine world: review and projection of warming-induced plant cover change in the Swedish Scandes. Ambio 39:159–169
Liseikin VD (2004) A computational differential geometry approach to grid generation. Springer, Berlin
MacEachren AM, Davidson JV (1987) Sampling and isometric mapping of continuous geographic surfaces. Am Cartogr 14:299–320
Malik SC, Savita A (1992) Mathematical analysis. New Age International Publishers, New Delhi
Marquinez J, Lastra J, Garcia P (2003) Estimation models for precipitation in mountainous regions: the use of GIS and multivariate analysis. J Hydrol 270:1–11
Ninyerola M, Pons X, Roure JM (2000) A methodological approach of climatological modeling of air temperature and precipitation through GIS techniques. Int J Climatol 20:1823–1841
Ninyerola M, Pons X, Roure JM (2007) Monthly precipitation mapping of the Iberian Peninsula using spatial interpolation tools implemented in a Geographic Information System. Theor Appl Climatol 89:195–209
Phillips DL, Dolph J, Marks D (1992) A comparsion of geostatistical procedures for spatial analysis of precipitation in mountainous terrain. Agric For Meteorol 58:119–141
Portales C, Boronat N, Pardo-Pascul JE, Balaguer-Beser A (2010) Seasonal precipitation interpolation at the Valencia region with multivariate methods using geographic and topographic information. Int J Climatol 30:1547–1563
Robertson AW, Ines AVM, Hansen JW (2007) Downscaling of seasonal precipitation for crop simulation. J Appl Meteorol 46:677–693
Rowhani P, Lobell BD, Linderman M, Ramankutty N (2011) Climate variability and crop production in Tanzania. Agric For Meteorol 151:449–460
Samanta S, Pal DK, Pal B, Lohar D (2012) Interpolation of climate variables and temperature modeling. Theor Appl Climatol 107:35–45
Sato YS, Yamashita F, Sugiura Y (2004) FIB-assisted TEM study of an oxide array in the root of a friction stirweided aluminum alloy. Scr Mater 50:365–369
Seo DJ (1996) Nonlinear estimation of spatial distribution of rainfall—an indicator cokriging approach. Stoch Hydrol Hydraul 10:127–150
Smith B, Prentice IC, Sykes MT (2001) Representation of vegetation dynamics in the modeling of terrestrial ecosystems: comparing two contrasting approaches within European climate space. Glob Ecol Biogeogr 10:621–637
Somasundaram D (2005) Differential geometry. Alpha Science International, Harrow
Teegavarapu RSV (2007) Use of universal function approximation in variance dependent interpolation technique: an application in Hydrology. J Hydrol 332:16–29
Thornton PE, Running SW, White MA (1997) Generating surfaces of daily meteorological variables over large regions of complex terrain. J Hydrol 190:214–251
Tong ST, Naramngam S (2007) Modeling the impacts of farming practices on water quality in the little Miami river basin. Environ Manag 39:853–866
Toponogov VA (2006) Differential geometry of curves and surfaces. Birkhaeuser, Boston
Vicente-Serrano SM, Saz-Sanchez MA, Cuadrrat JM (2003) Comparative analysis of interpolation methods in the middle Ebro Valley (Spain): application to annual precipitation and temperature. Clim Res 24:161–180
Vieux BE (2001) Distributed hydrologic modeling using GIS. Water Science and Technology Library. Kluwer Academic Publishers, Dordrecht
Wang F (2006) Quantitative methods and applications in GIS. CRC Press, Boca Raton
Xu CY, Singh VP (1998) A review on monthly water balance models for water resources investigations. Water Resour Manag 12:31–50
Yan H, Nix HA, Hutchinson MF, Booth TH (2005) Spatial interpolation of monthly mean climate data for China. Int J Climatol 25:1369–1379
Yue TX (2011) Surface modeling: high accuracy and high speed methods. CRC Press, New York
Yue TX, Du ZP (2006) High accuracy surface modeling and comparative analysis of its errors. Prog Nat Sci 16:986–991 (in Chinese)
Yue TX, Du ZP, Song DJ, Gong Y (2007) A new method of high accuracy surface modeling and its application to DEM construction. Geomorphology 91:161–172
Yue TX, Fan ZM, Chen CF, Sun XF, Li BL (2011) Surface modeling of global terrestrial ecosystems under three climate change scenarios. Ecol Model 222:2342–2361